Visible light mediated electrocatalytic activity in reduced graphene oxide supported bismuth ferrite

Ayan Mukherjee[1], Sankalpita Chakrabarty[1], Neetu Kumari[1], Wei-NienSu[2],Suddhasatwa Basu[1*]

[1]Department of Chemical Engineering, Indian Institute of Technology Delhi, New Delhi 110016, India

[2]NanoElectrochemistry Laboratory, Graduate Institute of Applied Science and Technology, National Taiwan University of Science and Technology, Taipei 106, Taiwan

Content

Total number of pages **17**

Total number of figures **09**

Total number of tables **04**

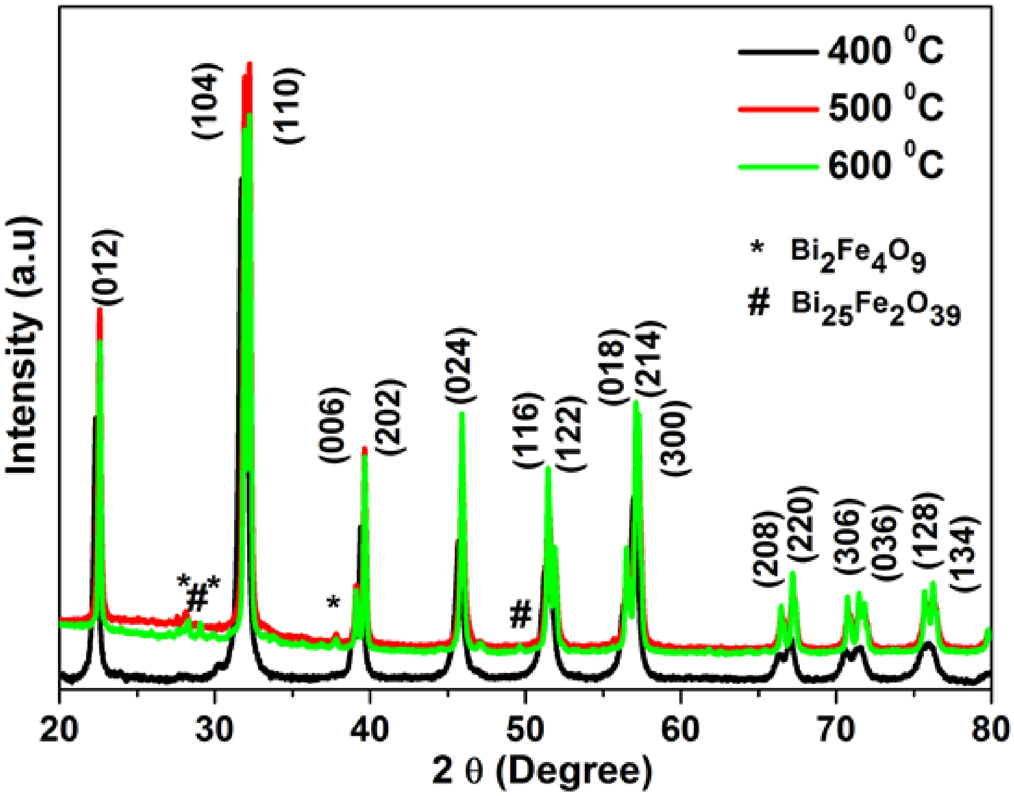

1.1 Figure S1 XRD pattern of BFO calcined at 400 °C, 500°C and 600°C

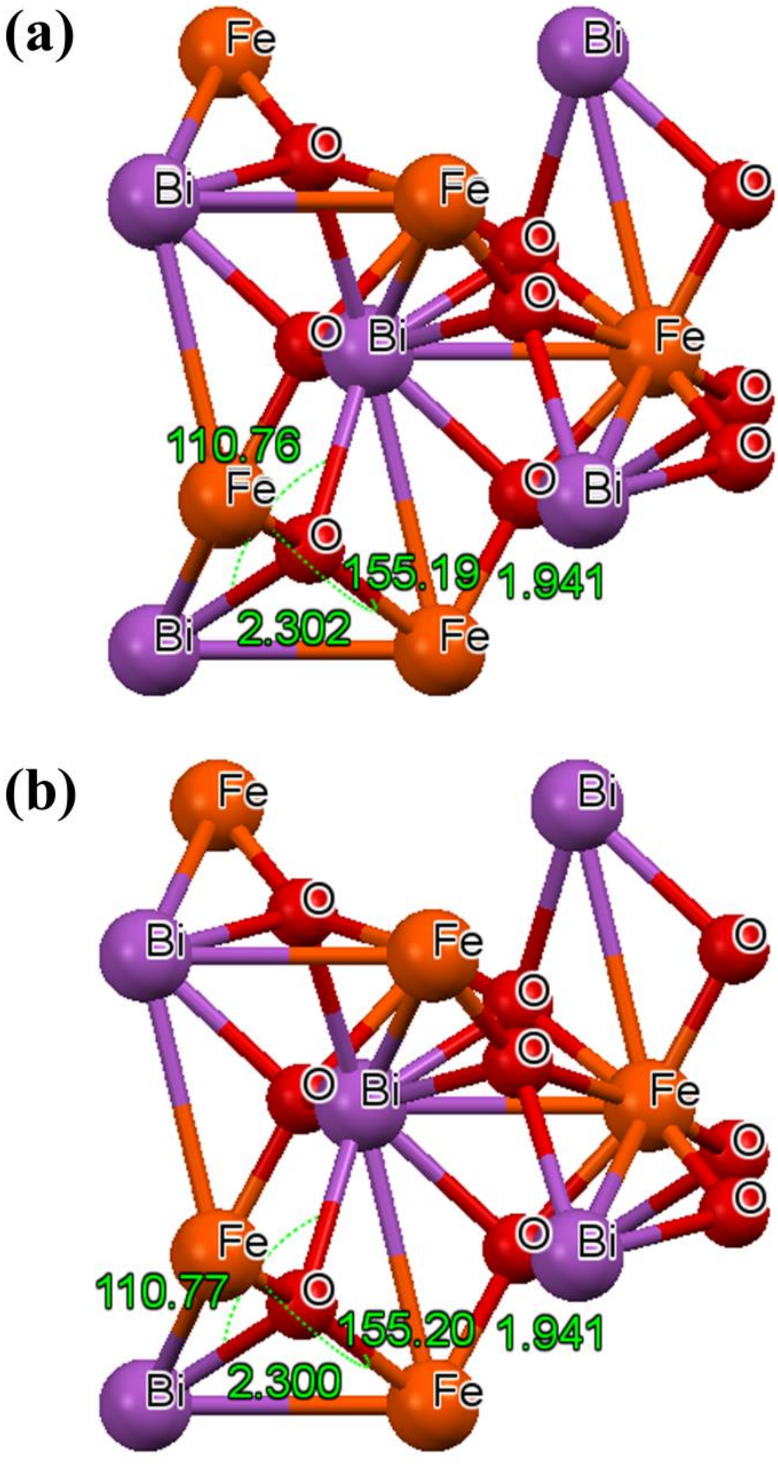

1.2 Figure S2 Rhombohedral cage of (a) BFO, (b) RGO-BFO

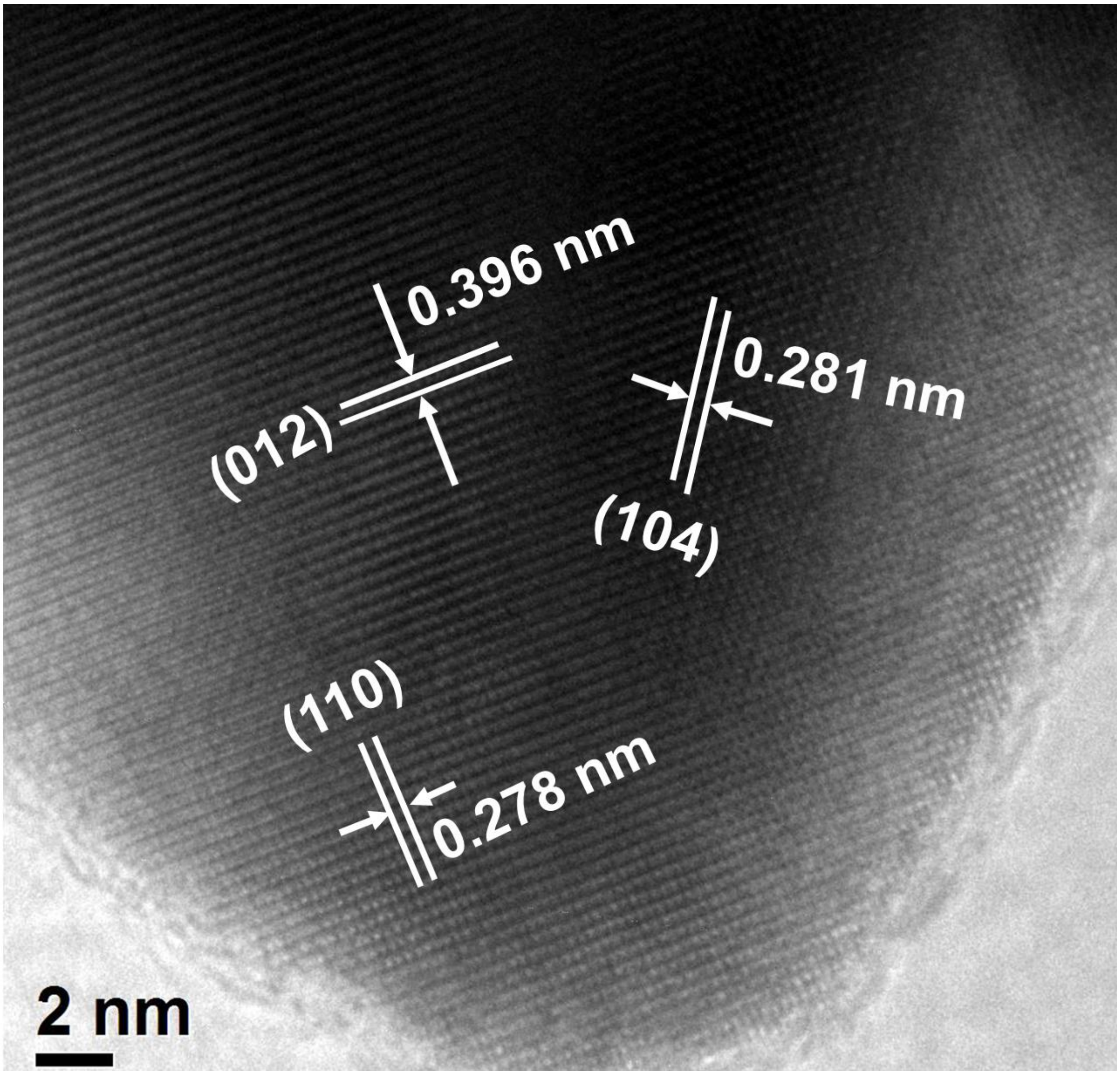

1.3 Figure S3 HRTEM image of BFO

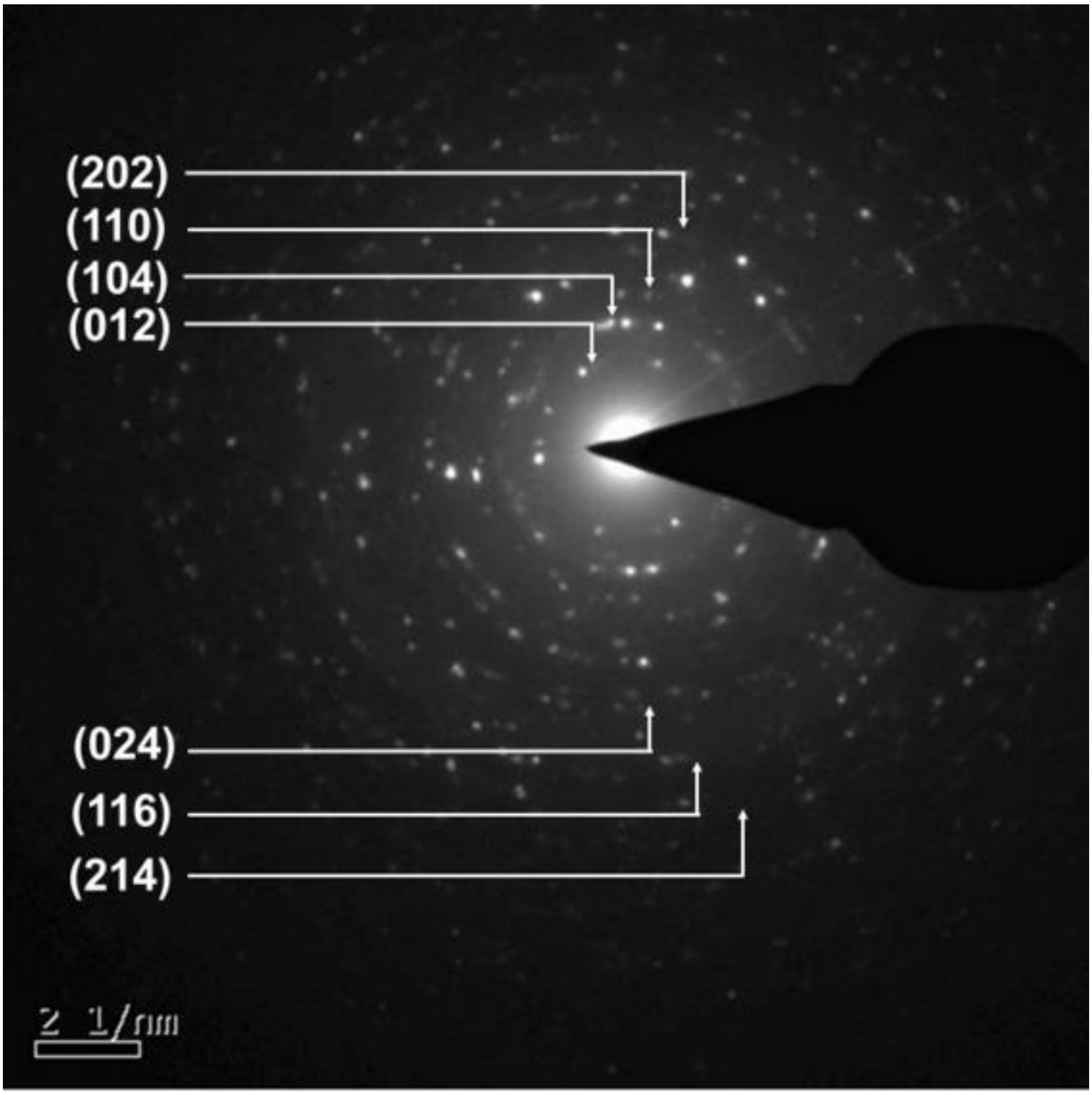

1.4 Figure S4 SAED pattern of BFO

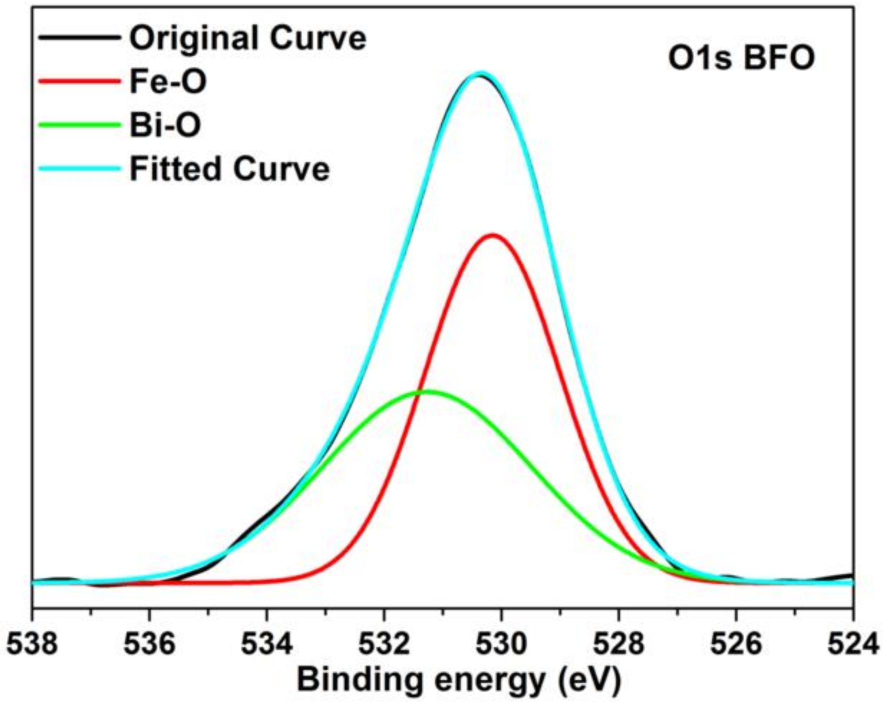

1.5 Figure S5 O1s core-level electron of BFO

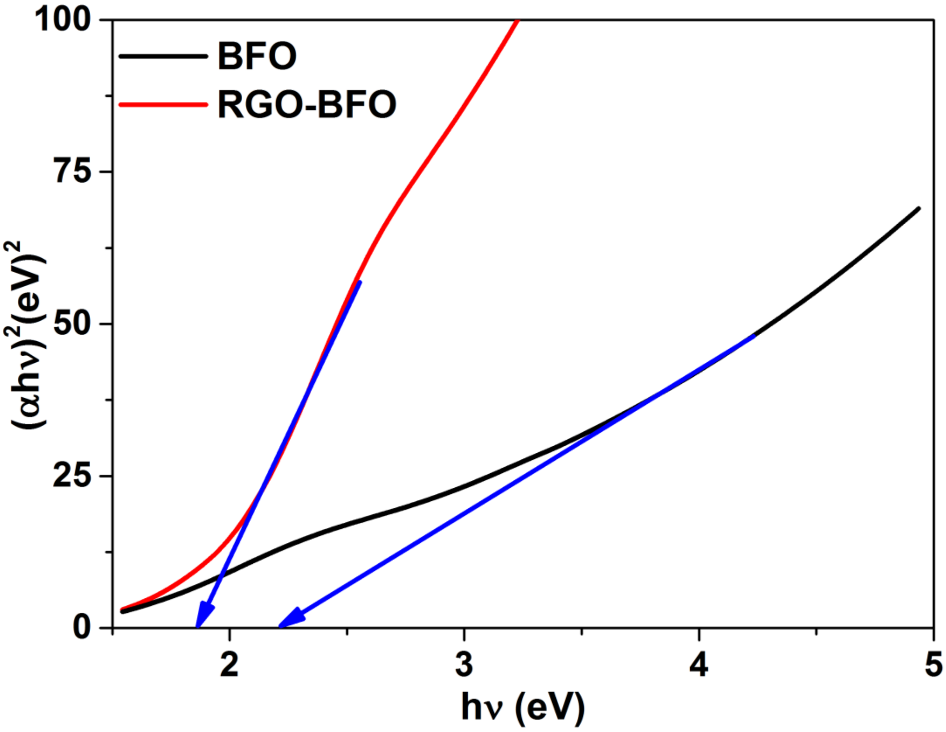

1.6 Figure S6 Tauc plot for determining band gap of BFO and RGO-BFO.

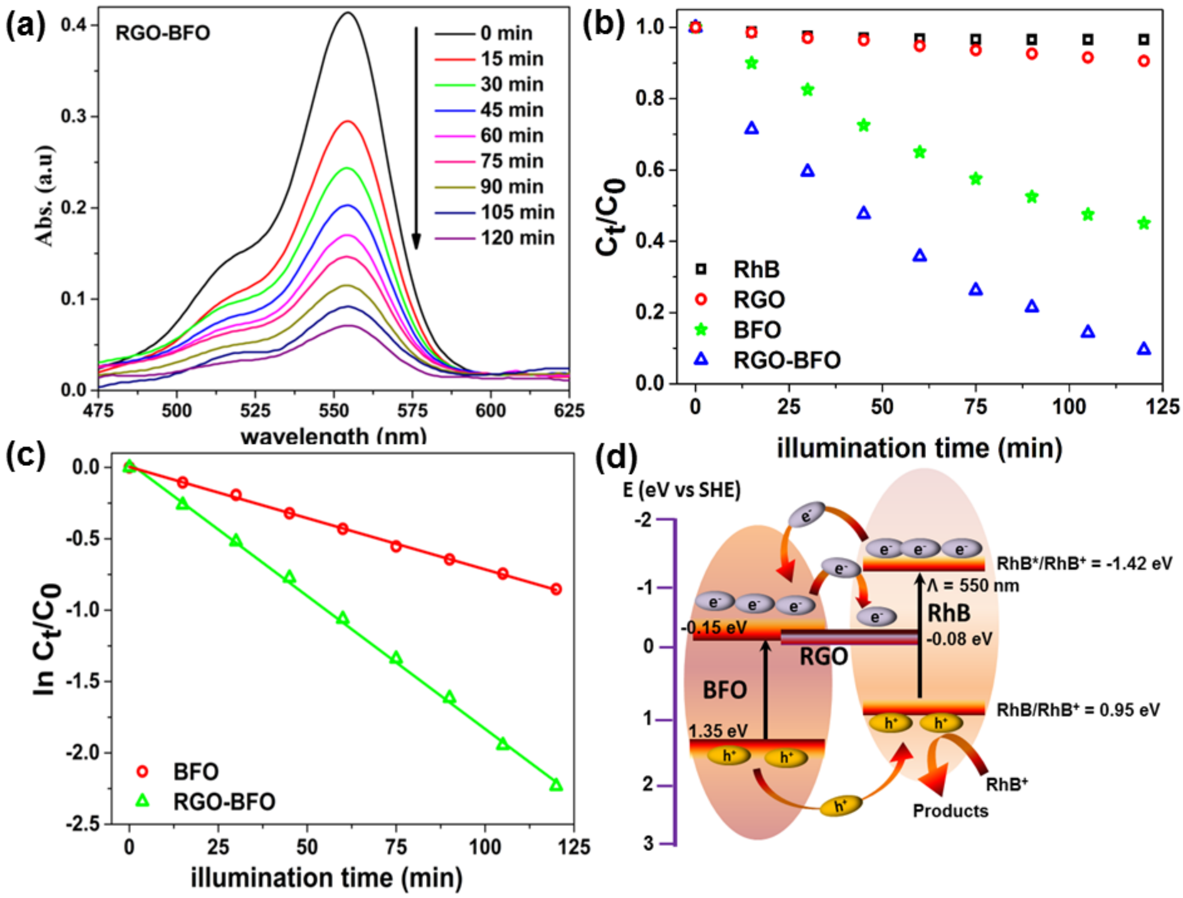

1.7 Figure S7 (a) Degradation of Uv-vis spectra of RhB over RGO-BFO, (b) Photocatalytic degradation efficiency of RhB without and withRGO-BFO, (c) Pseudo first order rate constant for the photodecomposition, (d) Energy diagram of RhB, RGO and BFO

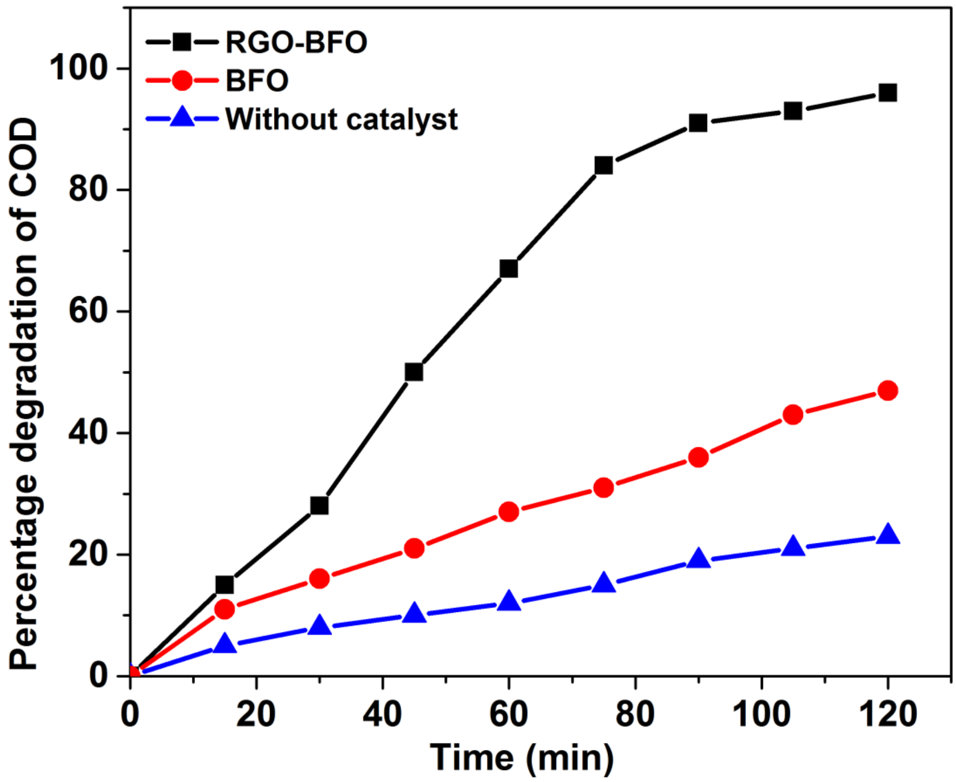

1.8 Figure S8 Percentage degradation of RhB dye in terms of COD values with time for different RGO and RGO-BFO

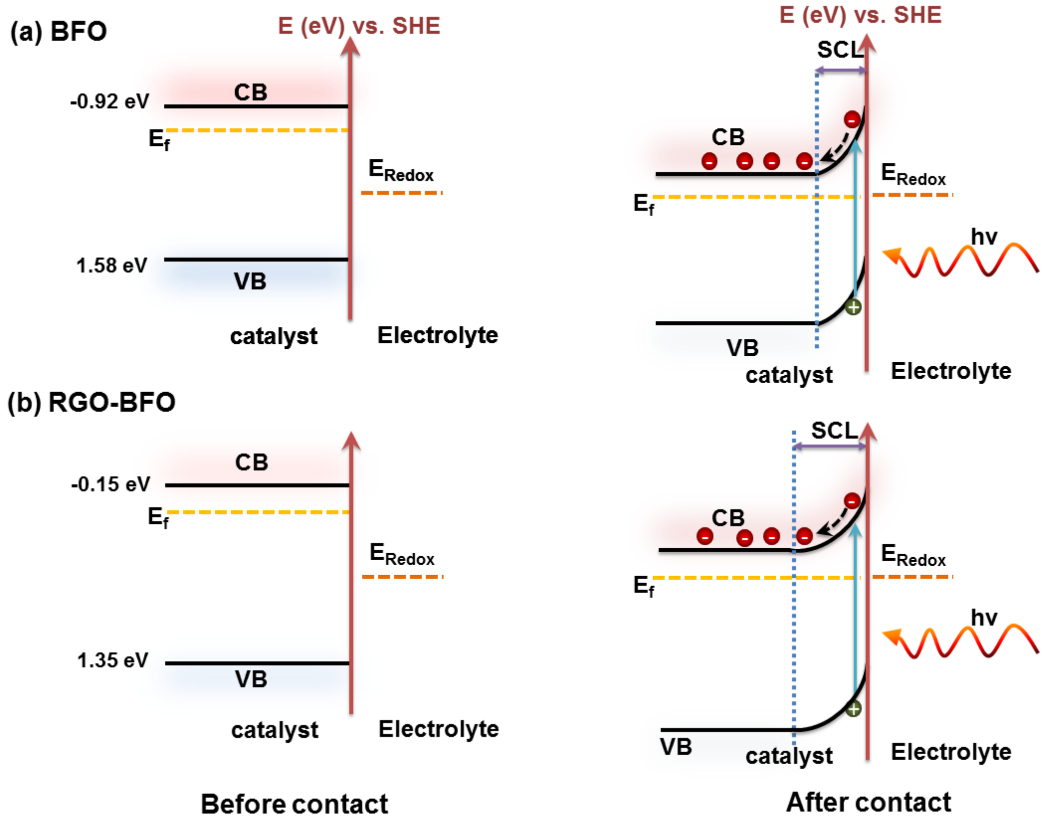

1.9 Figure S9 Schematic diagram of band bending for (a) BFO and (b) RGO-BFO in1M KOH electrolyte

1.10 Table S1 Reitveld refinement parameters of BFO and RGO-BFO

Sample		BFO	RGO-BFO
a (Å)= b (Å)		5.571 (6)	5.568 (8)
c (Å)		13.854 (8)	13.851 (7)
Cell Volume ($Å^3$)		372.36 (9)	371.72 (8)
Crystallite Size (nm)		20.2 (3)	18.8 (3)
MicroStrain x 10^{-3}		2.00 (2)	2.11 (4)
GOF (χ^2)		1.07	1.03
Bond lengths (Å)			
Fe-O		1.941	1.941
Bi-O		2.302	2.300
Bond Angles (°)			
Fe-O-Fe		155.19	155.20
Bi-O-Bi		110.76	109.77
Atomic Position			
x	Bi	0	0
	Fe	0	0
	O	0.4430 (8)	0.4428 (5)
y	Bi	0	0
	Fe	0	0
	O	0.0132 (9)	0.0128 (2)
z	Bi	0	0
	Fe	0.22216 (5)	0.22211 (6)
	O	0.9540 (6)	0.9535 (5)
R_{wp}		18.5	18.3
R_p		4.4	4.1
R_{Bragg}		5.1	4.7

1.11 Table S2. Various Raman modes observed in BFO

Position (cm^{-1})	115	123	157	180	197	214	230	270	477	534	606
Mode	E(TO1)	E(LO1)	A(LO1)	A(TO1)	A(LO2)	E(TO2)	A(TO2)	E(TO3)	E(TO4)	E(TO5)	E(TO6)

1.12 Table S3. Performance comparison of different catalysts including RGO-BFO for degradation of various organic contaminant.

Catalyst	Catalyst concentration ($mg.ml^{-1}$)	Contaminant	Degradation %	Degradation Time (min)	Rate constant	Ref
RGO-BFO	**0.33**	**RhB**	**91**	**120**	**1.86×10^{-2}**	**This work**
BFO/$(BiFe)_2O_3$	--	Gaseous Toluene	54	180	--	[1]
BFO/TiO_2	2	Congo Red	70	120	--	[2]
BFO/RGO	0.5	Bisphenol A	99	70	--	[3]
BFO/RGO	1	Congo Red	75	120	1.8×10^{-2}	[4]
10% Gd doped BFO	1	RhB	94	120	--	[5]
BFO/RGO	1	Congo Red	70	120	0.96×10^{-2}	[6]

1.13 Table S4. Performance comparison of various catalysts including RGO-BFO for Photoelectrochemical water splitting

Catalyst	Photocurrent density (mA.cm^{-2})	Onset potential (V)	STH %	Ref
RGO-BFO	**10.2 at 0.6 V (Ag/AgCl)**	**0.32 V (Ag/AgCl)**	**3.3**	**This work**
BFO	4.0 at 0.6 V (Ag/AgCl)	0.4 V (Ag/AgCl)	0.75	This work
$BiVO_4/TiO_2$	4.44 at 1.23 V (RHE)	-0.14 V (RHE)	2.87	[7]
CaFe2O4/TaON	1.26 at 1.23 V (RHE)	0.7 V (RHE)	0.55	[8]
Fe_2O_3/RGO/$BiV_{1-x}Mo_xO_4$	1.97 at 1 (Ag/AgCl)	0.33 V (Ag/AgCl)	0.53	[9]
A-Fe_2O_3/$NiMnO_x$	2.35 at 0.23 (Ag/AgCl)	-0.1 V (Ag/AgCl)	0.85	[10]
Co-Pi/ZFO/Ti:Fe_2O_3	3.6 at 1.23 (RHE)	0.85 (RHE)	0.33	[11]
RGO-MoS_2/$NiCo_2O_4$	5.36 at 0.8 V (Ag/AgCl)	0.1 V (Ag/AgCl)	3.08	[12]
Fe_2O_3-RGO	2 at 1.6 V (RHE)	0.88 V (RHE)	0.102	[13]
TiO2/RGO/NiFe	1.74 at 0.6 V (SCE)	-0.3 V (SCE)	0.58	[14]

References

(1) Kong, J.; Rui, Z.; Wang, X.; Ji, H.; Tong, Y. Visible-Light Decomposition of Gaseous Toluene over BiFeO 3 –(Bi / Fe) 2 O 3 Heterojunctions with Enhanced Performance. *Chem. Eng. J.***2016**, *302*, 552–559.

(2) Li, S.; Lin, Y.; Zhang, B.; Li, J.; Nan, C. BiFeO 3 / TiO 2 Core-Shell Structured Nanocomposites as Visible-Active Photocatalysts and Their Optical Response Mechanism. *J. Appl. phys.***2009**, *105*, 054310.

(3) Soltani, T.; Lee, B. Sono-Synthesis of Nanocrystallized BiFeO 3 / Reduced Graphene Oxide Composites for Visible Photocatalytic Degradation Improvement of Bisphenol A. *Chem. Eng. J.***2016**, *306*, 204–213.

(4) Li, Z.; Shen, Y.; Yang, C.; Lei, Y.; Guan, Y.; Lin, Y.; Liu, D.; Nan, C. Significant Enhancement in the Visible Light Photocatalytic Properties of BiFeO3–graphene Nanohybrids. *J. Mater. Chem. A***2013**, *1*, 823–829.

(5) Guo, R.; Fang, L.; Dong, W.; Zheng, F.; Shen, M. Enhanced Photocatalytic Activity and Ferromagnetism in Gd Doped BiFeO 3 Nanoparticles. *J. Phys. Chem. C***2010**, *114*, 21390–21396.

(6) Li, Z.; Shen, Y.; Guan, Y.; Hu, Y.; Lin, Y.; Nan, C.-W. Bandgap Engineering and Enhanced Interface Coupling of Graphene–$BiFeO_3$ Nanocomposites as Efficient Photocatalysts under Visible Light. *J. Mater. Chem. A***2014**, *2* (6), 1967–1973.

(7) Singh, A. P.; Kodan, N.; Mehta, B. R.; Held, A.; Mayrhofer, L.; Moseler, M. Band Edge Engineering in BiVO4/TiO2 Heterostructure: Enhanced Photoelectrochemical Performance through Improved Charge Transfer. *ACS Catalysis***2016**, *6* (8), 5311–5318.

(8) Kim, E. S.; Nishimura, N.; Magesh, G.; Kim, J. Y.; Jang, J. W.; Jun, H.; Kubota, J.; Domen, K.; Lee, J. S. Fabrication of CaFe2O4/TaON Heterojunction Photoanode for Photoelectrochemical Water Oxidation. *Journal of the American Chemical Society***2013**, *135* (14), 5375–5383.

(9) Hou, Y.; Zuo, F.; Dagg, A.; Feng, P. Visible Light-Driven a-Fe2O3 Nanorod/Graphene/BiV1- XMoxO4 Core/Shell Heterojunction Array for Efficient Photoelectrochemical Water Splitting. *Nano Letters***2012**, *12* (12), 6464–6473.

(10) Bhandary, N.; Singh, A. P.; Ingole, P. P.; Basu, S. Enhanced Photoelectrochemical Performance of Electrodeposited Hematite Films Decorated with Nanostructured NiMnO X. *RSC Adv.***2016**, *6* (42), 35239–35247.

(11) Chen, Y. J.; Chen, L. Y. The Study of Carrier Transfer Mechanism for Nanostructural Hematite Photoanode for Solar Water Splitting. *Applied Energy***2016**, *164*, 924–933.

(12) Chakrabarty, S.; Mukherjee, A.; Basu, S. RGO-MoS 2 Supported NiCo 2 O 4 Catalyst toward Solar Water Splitting and Dye Degradation. *ACS Sustainable Chemistry & Engineering***2018**, *6*, 5238–5247.

(13) Tamirat, A. G.; Su, W. N.; Dubale, A. A.; Pan, C. J.; Chen, H. M.; Ayele, D. W.; Lee,

J. F.; Hwang, B. J. Efficient Photoelectrochemical Water Splitting Using Three Dimensional Urchin-like Hematite Nanostructure Modified with Reduced Graphene Oxide. *Journal of Power Sources* **2015**, *287*, 119–128.

(14) Ning, F.; Shao, M.; Xu, S.; Fu, Y.; Zhang, R.; Wei, M.; Evans, D. G.; Duan, X. TiO_2 /Graphene/NiFe-Layered Double Hydroxide Nanorod Array Photoanodes for Efficient Photoelectrochemical Water Splitting. *Energy Environ. Sci.* **2016**, *9* (8), 2633–2643.